Reference: *Biol. Bull.* **187**: 293–299. (December, 1994)

Time-Resolved Imaging of Ca^{2+}-Dependent Aequorin Luminescence of Microdomains and QEDs in Synaptic Preterminals

ROBERT B. SILVER[1,3], MUTSUYUKI SUGIMORI[2,3], ERIC J. LANG[2,3], AND RODOLFO LLINÁS[2,3]

[1]*Section and Department of Physiology, Cornell University, Ithaca, New York 14853-6401,* [2]*Department of Physiology and Biophysics, New York University Medical Center, 550 First Avenue, New York, New York 10016, and* [3]*Marine Biological Laboratory, Woods Hole, Massachusetts 02543*

Localized elevation of intracellular free calcium $[Ca^{2+}]_i$ concentration serves as the trigger for a wide variety of physiological processes, e.g., *neurotransmitter release at most chemical synapses (1–3). The details of the mechanisms that regulate these processes are still unresolved (3–6), but they must involve precise temporal sequences of molecular events initiated by a transient localized elevation of Ca^{2+} concentration* (i.e., *a Ca^{2+} microdomain [3, 7–15]). A microdomain is defined as an autonomous compartment of minimal spatio-temporal volume within which a signaled process can occur (8, 10, 12). A quantum emission domain (QED) is a quantal signal element (3, 16, 17). The concept of a QED was first applied to Ca^{2+} signaling at the synaptic preterminal (3, 4) and for large-diameter mitotic cells (16, 17).*

The concept of Ca^{2+} microdomains was tested by labeling preterminals of squid giant synapses with low-sensitivity aequorin (a photoprotein that emits a photon upon binding Ca^{2+} [18, 19]). That work confirmed earlier modeling efforts (10, 16) and showed that, upon depolarization, the $[Ca^{2+}]_i$ profile reaches 200–300 μM within the microdomains, and that these $[Ca^{2+}]_i$ profiles are composed of groups of short-lived 0.5 μm diameter QEDs. In those records, obtained with 2:1 interlacing devices operating at the RS-170 standard, QEDs appeared as striped dots or chevrons rather than as solid dots, indicating that a QED lasted less than 16.6 ms (one video field), and thus establishing the need for higher sampling rates to better characterize the QED. In the present set of studies, we sought to extend our earlier work on calcium microdomains and QEDs with the goal of better understanding the lifetime of the QED and its relationship to the action potential. This is the first description of the methodology necessary to image the Ca^{2+} QED, and the techniques for obtaining, processing, and analyzing video information at high frame rates.

Received 20 September 1994; accepted 5 October 1994.

Portions of this work were presented in preliminary form at the General Scientific Meetings at the Marine Biological Laboratory, Woods Hole, MA, on 16 August 1994.

Abbreviations: CCD = charge coupled device; dMCP = dual microchannel plate image intensifier; N.A. = numerical aperture; NTSC = National Television Standards Committee; QED = quantum emission domain; RS-170 = NTSC Resolution Standard 170: video frame resolution of 525 lines of horizontal resolution, 60 Hz video field sampling rate, 2:1 interlace of video fields within a single video frame, 33 ms per frame (16.66 ms per video field); used primarily for black and white video devices.

Chevrons and dots in interpreting the duration of QEDs

QED patterns in aequorin-labeled synaptic preterminals were observed as discrete events following stimulation of single action potentials. These observations were initially performed at a video frame rate of 30 frames per second (fps), using cameras conforming to the RS-170 standard. Each video frame consisted of two interlaced video fields (*i.e.*, 2:1 interlace), each composed of the set of odd or even scan lines. A new field was captured every 16.7 ms, and each scan line lasted for 63.5 μs. Therefore, an event lasting 16.7 to 33 ms would be seen as a solid dot, while one lasting less than 16.7 ms would be observed as a set of horizontal stripes. Events of duration close to 16.7 ms might also appear as dots, depending upon the timing of the initiation of the event relative to the timing of the two video fields. If the event began close to the end of the first

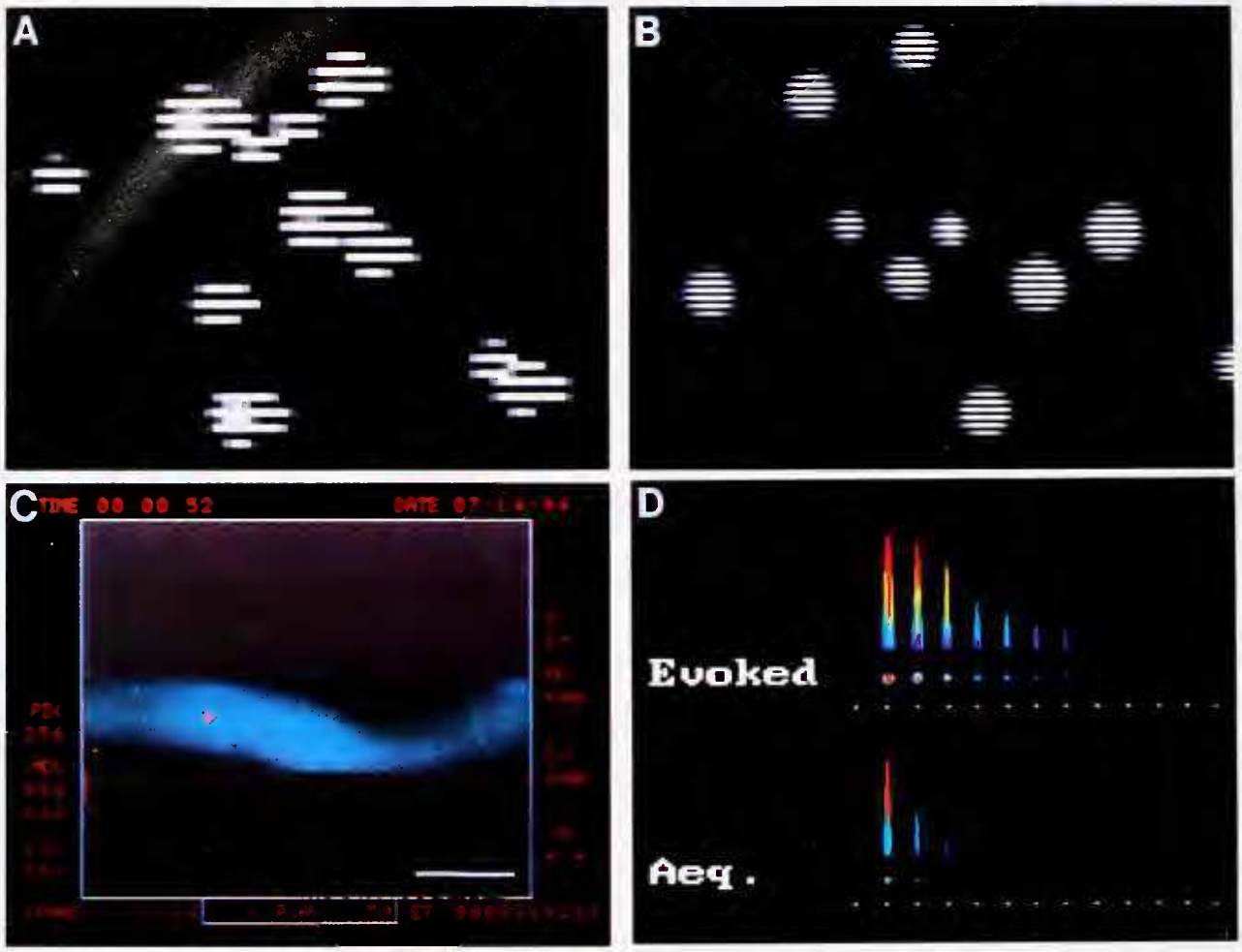

Figure 1. (A) Individual quantum emission domains (QEDs) activated by single action potentials at a preterminal appear as white chevrons when recorded at 30 frames per second (fps). A few of these QEDs show some filling between the stripes, indicating that those events began close to either the start or end of a single video field and overlapped to the preceding or following video field. The two QEDs seen in the lower right of this panel occurred in separate odd and even fields. (B) Individual QEDs activated by single presynaptic spikes appear as white chevrons recorded at 200 fps, indicating that the entire QED occurred within the 2.5-ms sampling period of the video field. Note that in this case, unlike that in panel A, all of the QEDs appear as chevrons, indicating that no observed QEDs overlapped two consecutive video fields. (C) The first 0.25-ms video frame recording of a single evoked QED (red) superimposed onto its point of origin in a synaptic preterminal (blue). The red characters surrounding the central image are typical of the display from the Kodak high-speed video camera. (D) The time course of an evoked QED, and one for a single QED emitted from aequorin expressed into calcium buffer, recorded at a video rate of 4000 fps. Spots of light from single video frames are displayed as a row of spots at the same horizontal level as the terms "Evoked" and "Aeq." The intensity profiles of each of the individual spots are seen directly above their respective spots. The spots and intensity profiles were printed in pseudocolor to aid in visualization; black and purple are 0 to low intensity, increasing through green, yellow, and orange to the highest values of red and white (8-bit gray-scale value of 255). These values are correlated with the luminance intensity incident to the faceplate of the dual microchannel plate (dMCP) intensifier. Small white points marking each individual video field appear below their respective spots. The scale marker in panel C represents 10 μm.

Standard methods were used to dissect stellate ganglia from small squid (*Loligo pealei*) and monitor synaptic transmission (3, 18). Video images were captured with a direct optical extension onto a dMCP Video Intensified Microscopy camera system (Hamamatsu Argus 100; Hamamatsu Photonics, Inc., Bridgewater, NJ) operated in photon-counting mode. Three different video cameras were used to detect clouds of electrons emanating from the dMCP. For video at 30 fps, a Hamamatsu saticon tube camera was used, operated under the RS-170 standard. Imagery from the saticon camera was recorded on an S-VHS videocassette recorder. An NAC HSV-400 (NAC, Inc., Japan) high-speed color video camera, S-VHS videocassette recorder, and Panasonic ST-1000 color video monitor (Matsushita Electric Industrial Co., Ltd., Fukuoka, Japan), all operated in B/W mode, were used for 200-fps imaging and recording. The NAC HSV-400 camera was fitted to the dMCP through a direct optical coupling. Care was taken to ensure that the output image of the dMCP

video field or ended near to the start of the second video field, the event would be recorded as a partially filled chevron whose centroid coincided with the location of the point of origin for the event. Events that were very short compared with the video-field sampling rate would nearly always appear as chevrons. This principle applies to all 2:1 interlaced imaging devices, irrespective of video frame rate.

QED images at 30 video frames per second

$Ca^{2+}{}_i$-dependent aequorin luminescence was detected as discrete QEDs at the preterminal side of the synapse following presynaptic action potentials (Fig. 1A). Because QEDs were seen as chevrons, rather than solid spots, they must have had a lifetime of less than 16.7 ms; nearly all of the presynaptic QEDs observed after such action potentials appeared as chevrons. In several instances, chevron QEDs were seen to interlace. These were fortuitous observations, and would be expected for near-neighboring QEDs acting within microdomains. In several other instances, some of the QED signal extended to the following (or from the preceding) video field; that is, the blank space between the lines of the chevrons contained some record of a signal. We interpret these images to represent a short-lived event that occurred near the end (or beginning, respectively) of a given video field that contained the majority of the chevron QED photon emission.

QED images at 200 video frames per second

Because virtually all of the QEDs observed at 30 fps appeared on the video monitor as chevrons, better temporal resolution was clearly needed. To resolve individual QEDs in time, aequorin luminescence was videotaped at 200 fps (5-ms video frame, 2.5 ms per video field). Fig. 1B shows examples of QEDs recorded at a frame rate of 200 fps from a single evoked response. As at 30 fps, they appeared as chevrons, so their lifetime must be less than 2.5 ms. Moreover, fewer than 5% of the QEDs were seen as partially filled chevrons, indicating both that the event was less than the video frame rate and that no significant degree of overlap occurred in which QEDs "began" in one 1.25-ms video field and then extended into the next.

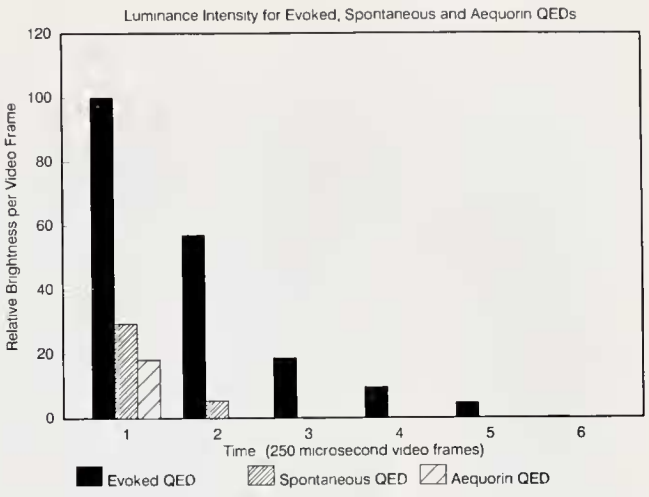

Figure 2. Luminance intensity for evoked, spontaneous, and aequorin QEDs corrected for phosphorescent afterglow. Values are means of the total luminance intensity for each of five QEDs for each category, and are expressed as relative to the brightness of the initial frame of an evoked QED. Evoked QEDs (solid black) lasted as long as five 0.25-ms video frames; mean spontaneous QEDs (thin double stripes) lasted only 0.5 ms; and aequorin QEDs (single diagonal crosshatches) were seen for only one 0.25-ms video frame.

To ensure that the imagery information was properly processed, the following assumptions and practices were adopted. The photon intensity information of the initial video frame recording a QED was considered to represent light from the photochemical reaction of Ca^{2+} and aequorin. The contribution of afterglow in the first video frame of each QED record was considered to be negligible for imagery at 4000 fps. Image information for each subsequent frame was considered to consist of a sum of the Ca^{2+}-dependent aequorin-based photon emission generated and integrated onto the detector faceplate during that video frame, and the afterglow attributable to the preceding video frame. The contribution of afterglow was determined with empirical values derived from the images for aequorin injected into Ca^{2+}-containing buffer as follows. The luminance intensity values for QED photon emissions from each 0.25-ms video frame were determined from digitized video records. Photon emission from the reaction of Ca^{2+} and aequorin was assumed to last 0.25 ms, or possibly less; so additional light detected by the CCD camera was considered to be due to afterglow of the dMCP. The ratio of the total intensity of the second frame divided by the preceding frame was taken as the proportion of the total luminance intensity of the first frame assignable as afterglow in the second frame.

These results indicate that a further increase in video sampling rate would be needed to resolve the images of individual QEDs.

was focused to the faceplate of the camera. Higher speed digital video imagery was obtained with a Kodak Ektapro high-speed video system (Hi-Spec Processor and SI camera) operated at various frame rates between 30 fps and 4000 fps. High frame rate recordings were performed with reduced frame size; *e.g.*, the center 64 × 256 pixel region of the field of view at 4000 fps. The Kodak SI camera and video processor combination was selected as the detector of choice behind the Hamamatsu dMCP, for its flexibility in video frame rates, the linear performance characteristics of the charge coupled device (CCD) used in this camera, and an added advantage that every image recorded by the CCD was a single, non-interlaced frame. Video imagery was recorded in S-VHS format on 3M ST 120 Master Broadcast Videocassettes (3M Corp., Minneapolis, MN). Hard-copy video prints were produced with a Kodak SV 6510 color video printer (Eastman Kodak, Inc., Rochester, NY).

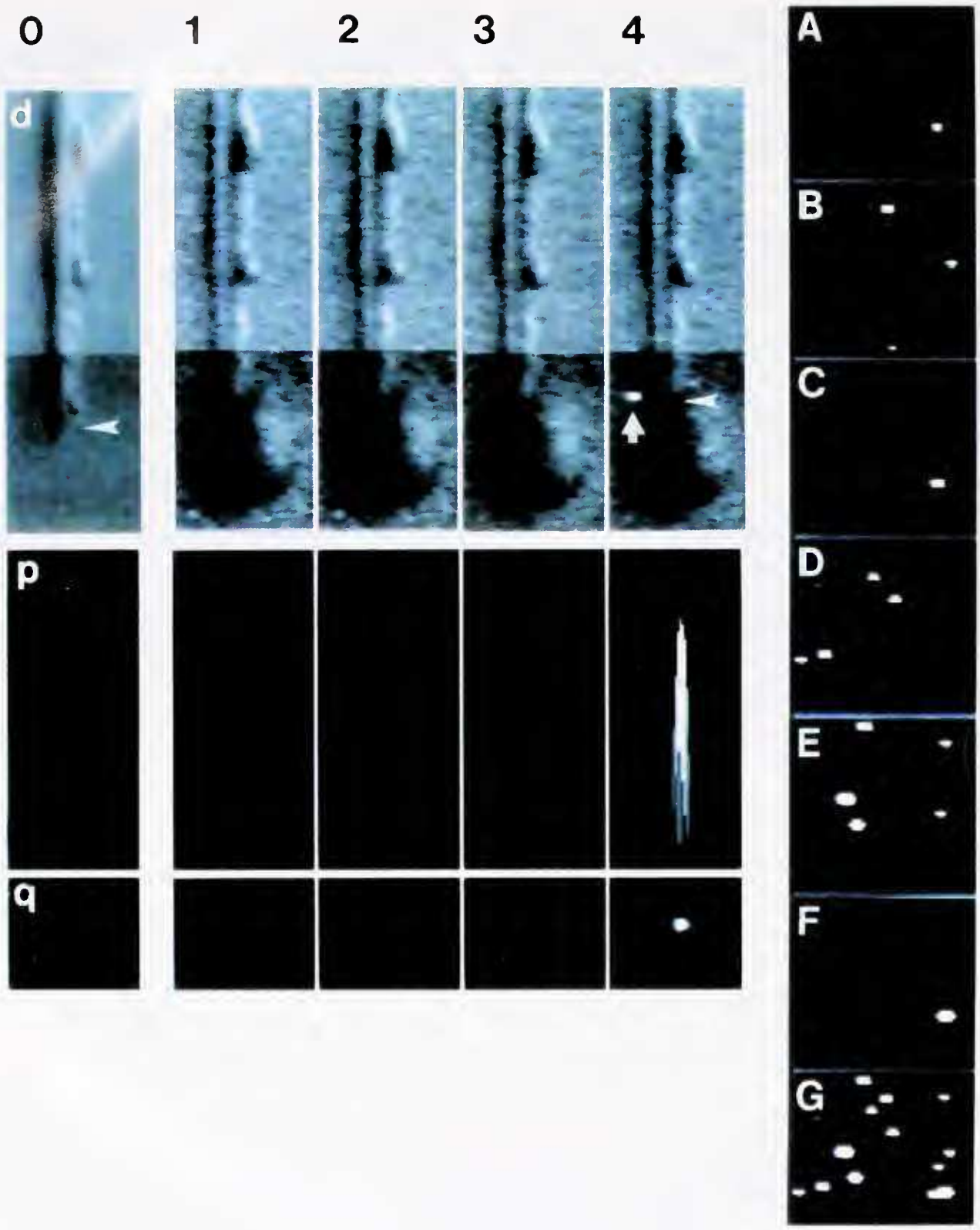

Figure 3. A recording of the time course of the calcium-dependent photon emission by aequorin. Columns 1 through 4 show images from single sequential 0.25-ms video frames from the 4000-fps video record. Column 0 shows an image obtained before the injection of aequorin. Row "d" shows the microinjection pipette using differential interference contrast (DIC) optics. Row "p" shows the linear intensity profile for each individual video frame corresponding to the DIC images in row "d" (above) and row "q" (below).

QED images at 4000 video frames per second

At 4000 fps, individual QEDs from within a stimulated preterminal were observed and recorded as sets of solid spots whose luminance intensity increased from background to maximum in the first frame and decreased in intensity with subsequent frames (Fig. 1C and D). Each QED record was preceded by a dark region (no light). The first frame of each QED showed a dramatic increase in luminance intensity, which resembled a symmetric dome of light distributed over an area less than 0.5 μm in diameter. Subsequent 0.25-ms video frames showed symmetrical domes with the same center as the first dome, but with less overall intensity. Each subsequent corrected frame decreased in intensity by a factor that seemed to follow an exponential decay curve (Fig. 2 and Table I).

Time-resolved imaging of aequorin luminescence in vitro

Any analysis of the QED images would require that we determine the time course for the aequorin reaction itself under the experimental conditions used. Published values for the lag time between the addition of Ca^{2+} to a solution of aequorin in a test tube and the emission of photons range between 2 and 10 ms (20, 21). That range is clearly too imprecise, so we sought a direct measurement using 4000-fps video, the imaging system being used for the experiments.

When aequorin was injected into Ca^{2+}-containing buffer, time-resolved Ca^{2+}-dependent aequorin luminescence could be detected with the dMCP-SI camera system operated at 4000 fps (Figs 1D and 3). Prior to the injection, the region around the tip of the micropipette appeared black; 0.75 ms after injection, bright spots of light appeared. Following the initial and rapid rise in luminescence, the signal diminished in intensity to background over a period of four or five 0.25-ms video frames. In six trials, 0.75 ms elapsed between the initial mixing of aequorin and Ca^{2+} buffer and the onset of photon emission. Thus, the intensity of Ca^{2+}-dependent aequorin luminescence was adequate to elicit a readily discernible signal from the dMCP-SI camera.

Shot noise

Shot noise was observed in recordings performed at all frame rates used in this study. In observations performed at 30 fps to 200 fps, shot noise appeared as a chevron. At 4000 fps, shot noise appeared as a bright spot lasting for one video frame (Fig. 1D). The intensity of these spots was typically less than 5% of the initial frame for a real QED.

Corrections of 4000 fps images for afterglow of faceplate phosphors

We applied arithmetic corrections to the raw QED images to compensate for the phosphorescent afterglow (22,

---

Row "q" shows the spots of light recorded as QEDs. Panel 1d corresponds to the same time period as shown in panels 1p and 1q; similarly 2d, 3d, and 4d correspond to 2p and 2q, 3p and 3q, and 4p and 4q, respectively. Panel 0d shows a 16-frame average of the oil- and aequorin-filled micropipette prior to injection of aequorin into the calcium buffer. Panels 0p and 0q show the corresponding intensity profile and QED record; *i.e.*, an absence of aequorin-mediated photon emission. The tip of the micropipette is noted with a horizontal, left-pointing arrowhead in this panel and panel 4d. Column 1 shows the first video frame following injection of aequorin into the calcium buffer. The micropipette in 1d is seen to be empty of the oil used to protect the aequorin from the calcium buffer prior to the injection. The oil droplet formed at the tip of the micropipette is seen as a sphere at the micropipette tip. Subsequent columns show the time course of the aequorin reaction, to the emission of the first QED (column 4).

Separately, panels A through F show an image integration of the first millisecond of QED emissions detected after injection of aequorin into calcium buffer for each of six separate experiments. The QED seen in panel C corresponds to the QED seen in panel 4d. Panel G shows an image integration of all of the QEDs detected in panels A through F. Note the high degree of spatial clustering of these initial QEDs recorded during one millisecond about the tip of the pipette.

To determine the lag time between the mixing of aequorin and Ca^{2+}, aequorin solutions were injected into Ca^{2+} buffers as previously described (3), and the reaction sequence was observed at 4000 fps. The method of injection of aequorin into the Ca^{2+} buffer was essentially identical to quantitative microinjections routinely performed (3, 19). For these experiments a multi-spectral video microscope was used (*e.g.*, 16, 17; developed by R. B. S.). The time of mixing was considered to have begun when the trailing meniscus of the first oil droplet was expressed from the tip of the pipette. Timing of the injection was coordinated with clock time of the video system. To assist in QED feature extraction and quantification, video images were processed, filtered, and analyzed with an Image1-AT (Universal Imaging Corp., West Chester, PA) running on a Dell 325 AT-bus computer, with macro programs written by one of us (R. B. S.). Ca^{2+},-dependent aequorin luminescence images of QEDs, seen as discrete spots on a dark background, were digitized and analyzed for each sequential video frame. The phosphorescent afterglow of the cameras and dMCP combinations contributes to the QED imagery (22, 23). The afterglow is due to the prolonged emission of energy from phosphors at the detector faceplate and is common to all phosphor-based image detectors. The afterglow and the contribution of shot noise to the imagery data are considered in the text and in Figure 2.

Table I

Mean luminance values and decay function attributes for individual evoked and spontaneous QEDs from synaptic preterminals and for aequorin QEDs produced in vitro

Event (*N*)	Video frame one mean intensity	Percent of frame one luminance intensity	Best curve fit[1]	Curve attributes		
				a	b	R^2
Evoked (5)	22096	100.0	Exponential[2]	51502.3	−0.79	0.9909[3,4]
Spontaneous (5)	6491	29.4	Exponential[2]	36106.5	1.72	—[5]
Aequorin (5)	4027	18.2	Square pulse of 0.25 ms[6]			

[1] Solutions for best fit (highest value for R^2) were sought using linear, exponential, logarithmic and power curve fit models.

[2] The curve is described by the equation $y = ae^{bx}$.

[3] Curve calculated using values from five points: frames 1 through 5 having luminance intensity values greater than 0.

[4] Numerical analyses of the imagery data were performed within the Image 1-AT and Lotus 1-2-3 Version 3.0 environments using macro programs written by one of us (R.B.S.). Curve fit analyses were performed with an HP-41cv calculator (Hewlett-Packard, Corvallis, OR).

[5] No value is reported here because only two values could be used to solve the curve.

[6] Square pulse assumed given single frame lifetime following application of correction for phosphorescent afterglow.

23) of the dMCP faceplate (see figure legends). Quantitative data related to the corrected QEDs from the evoked and spontaneous responses from synaptic preterminals and from photon emission from aequorin injected into Ca^{2+} buffer are summarized in Table I.

Upon analysis, the processed image data showed that (a) the mean evoked response followed an exponential decay profile that was no longer than 1.25 ms; (b) in more than 90% of the observed cases, the maximum emission intensity was achieved in the first video frame; (c) in the first frame, the peak intensity for spontaneous events reached a value only 18.2% of that achieved for evoked responses; (d) as resolved at 4000 fps, the mean spontaneous response followed an exponential decay profile and lasted for no more than 0.5 ms; (e) evoked QEDs were about five times more intense than spontaneous QEDs; and (f) the aequorin response was a square pulse lasting at most 0.25 ms.

Discussion

Here we compare time-resolved video images of Ca^{2+}-dependent aequorin luminescence *in vitro* and in a synaptic preterminal, at frame rates from 30 to 4000 fps. Calcium microdomains and quantum emission domains (QEDs) in synaptic preterminals and QEDs emitted by aequorin reacting with calcium buffers *in vitro* with the photoprotein *n*-aequorin-J. These photon emissions were highly localized in time and space. Clues to the ultimate speed and duration of aequorin-mediated photon emissions in control and experimental systems came from the appearance of the spots of light viewed on the video monitors: namely the chevrons. Images obtained at 30 fps and 200 fps showed the QEDs as chevrons, rather than solid spots, indicating that QED lifetime was less than the duration of a single 200-fps video field (2.50 ms). Images at 4000 fps revealed the time course for calcium entry to the synaptic preterminal for both evoked and spontaneous events, as well as for the reaction of aequorin with calcium *in vitro*. Corrections for phosphorescent afterglow of the camera were developed and applied to the video records; they revealed that evoked and spontaneous events last a maximum of 1.25 and 0.5 ms, respectively; evoked QEDs had a fivefold greater intensity than spontaneous events. The reaction of aequorin with calcium *in vitro* occurred about 0.75 ms after the aequorin and calcium were mixed, and lasted 0.25 ms or less. The calcium concentration profiles are presented for evoked and spontaneous QEDs in synaptic preterminals *in vivo* and for aequorin reacting with calcium *in vitro*. The very rapid events reported here match earlier accounts of rapid, localized calcium currents at active zones during transmitter release.

In the application of a dMCP for photon-limited specimens, it is important to recall how the intensified image is produced and what the image represents (24): a cloud of electrons proportional to the number of photons produced in the microchannels and presented to the faceplate of the camera is used to produce the final image. The dMCP photocathode exhibits a 10% efficiency, and 60% of the output of that photocathode is sampled by the open area of the microchannels of the dMCP (24). Thus only 6% of the incident photons are available to be amplified by the dMCP. The 40×, 0.75 N.A. objective lens used in these studies is about 92% efficient at 465 nm, with a sampling cone angle of 38.8° (Ms. Becky Hohman, Carl Zeiss, Inc., pers. comm.); therefore, that objective lens can collect only 3.7% of the photons emitted from a single photon point source exhibiting 4π radiation. Thus, a system composed of that objective lens and dMCP exhibits a 0.022% efficiency for each 4π photon produced by the Ca^{2+}-dependent aequorin luminescence. For the observation system used in these experiments, the probability of detecting a photon emitted from a Ca^{2+}-aequorin complex acting as a point source is no greater than 2.22

$\times 10^{-3}$. This number is very small, but it represents a realistic estimate of the state of the art of optical components available for imaging single photon and photon-limited events.

When extending observations to high-speed video, the operational relationship between available light, detector sensitivity, and frame rate of the camera must be considered. Within the spectral sensitivity band of the detector, observed image intensity is dependent upon the number of photons interacting with the detector in a sampling period. This is a consideration long known to those using high-speed photographic emulsions at low light levels—for example, in photomicrography of fluorescent specimens. In practice, the faster the frame rate, the less light available per image frame: as the frame rate doubles, the light available for an image is halved. At 200 fps the light available per frame is roughly 7^{-1} of that available at 30 fps; at 4000 fps the light available per video frame is 132^{-1} of that available at 30 fps. At 4000 fps we are, at best, able to detect only 1.7×10^{-5} photons emitted from the specimen in a single 0.25-ms video frame.

This paper reports time-resolved images of Ca^{2+} entry to the synaptic preterminal for evoked and spontaneous events within microdomains. From the measurements of the reaction lag time and duration of the aequorin reaction *in vitro*, it also appears that high-speed video is an effective tool for the study of molecular reactions in solution. The implications of these observations for synaptic physiology are discussed in the accompanying paper (18).

Acknowledgments

We thank Drs. O. Shimomura, S. Inouye, B. Musicki, and Y. Kishi for the generous gifts of the custom aequorin preparations used in this study. Thanks are also extended to Mr. Paul W. DelGrego (Motion System Analysis Division, Eastman Kodak Co.) for his assistance with the digital high-speed video observations, and to Ms. Becky Hohman and Mr. Phil Presley (Carl Zeiss, Inc.) for information regarding the characteristics of the objective lens used for observations of photon emissions *in vivo*. This work supported by the N. I. H. (NS 13742 to R. L.), the U. S. Air Force (F49620-92-J-0363 to R. L.), and the N. S. F. (DCB-9005343 and DCB-9308024 to R. B. S.).

Literature Cited

1. **Katz, B. 1969.** *The Release of Neurotransmitter Substances.* The Sherrington Lectures X. Thomas, Springfield, IL.
2. **Llinás, R. R. 1977.** Pp. 139–160 in *Approaches to the Cell Biology of Neurons,* Vol. 2, C. W. M. Ferendelli and J. A. Ferendelli, eds. Soc. for Neurosciences, Bethesda, MD.
3. **Llinás, R., M. Sugimori, and R. B. Silver. 1992.** Microdomains of high calcium concentration in a presynaptic terminal. *Science* **256:** 677–679.
4. **Llinás, R., M. Sugimori, and R. B. Silver. 1991.** Imaging preterminal calcium concentration microdomains in the squid giant synapse. *Biol. Bull.* **181:** 316–317.
5. **Llinás, R., M. Sugimori, and R. B. Silver. 1993.** Presynaptic calcium concentration microdomains and transmitter release. *J. Physiol. (Paris)* **86:** 135–138.
6. **Llinás, R., M. Sugimori, and R. B. Silver. 1994.** Localization of calcium concentration microdomains at the active zone of the squid giant synapse. Pp. 133–137 in *Molecular and Cellular Mechanisms of Neurotransmitter Release,* L. Stjärne, P. Greengard, S. Grillner, J. Hökfelt and D. Ottoson, eds. Raven Press, New York.
7. **Llinás, R. R., I. Z. Steinberg, and K. Walton. 1981.** Relationship between presynaptic calcium current and postsynaptic action potential in squid giant synapse. *Biophys. J.* **33:** 323–351.
8. **Chad, J. E., and R. Ekert. 1984.** Calcium domains associated with individual channels can account for anomalous voltage relations of Ca-dependent responses. *Biophys. J.* **45:** 993–999.
9. **Simon, S. M., M. Sugimori, and R. R. Llinás. 1984.** Modeling the submembranous calcium-concentration changes and their relation to rate of presynaptic transmitter release in the squid giant synapse. *Biophys. J.* **45:** p264a.
10. **Simon, S. M., and R. R. Llinás. 1985.** Compartmentalization of the submembrane calcium activity during calcium influx and its significance in transmitter release. *Biophys. J.* **48:** 485–498.
11. **Fogelson, A. L., and R. S. Zucker. 1985.** Presynaptic calcium diffusion from various arrays of single channels. *Biophys. J.* **48:** 1003–1007.
12. **Zucker, R. S., and A. L. Fogelson. 1986.** Relationship between transmitter release and presynaptic calcium influx when calcium enters through discrete channels. *Proc. Natl. Acad. Sci. U.S.A.* **83:** 3032–3036.
13. **Llinás, R., I. Z. Steinberg, and K. Walton. 1981.** Presynaptic calcium currents in squid giant synapse. *Biophys. J.* **33:** 289–321.
14. **Pumplin, D. W., T. S. Reese, and R. Llinás. 1981.** Are the presynaptic membrane particles the calcium channels? *Proc. Natl. Acad Sci. U.S.A.* **78:** 7210–7213.
15. **Pumplin, D. W., and T. S. Reese. 1978.** Membrane ultrastructure of the giant synapse of the squid *Loligo pealei*. *Neuroscience* **3:** 685–696.
16. **Silver, R. B. 1994.** Video light microscopic imaging of the calcium signal that initiates nuclear envelope breakdown in sand dollar (*Echinaracnius parma*) cells. *Biol. Bull.* **187:** 235–237.
17. **Silver, R. B., A. P. Reeves, M. Whitman, and B. Kelley. 1994.** Analysis of spatial and temporal patterns in the Ca^{2+} signal that signals nuclear envelope breakdown in sand dollar (*Echinaracnius parma*) cells. *Biol. Bull.* **187:** 237–238.
18. **Sugimori, M., E. J. Lang, R. B. Silver, and R. Llinás. 1994.** High-resolution measurement of the time course of calcium-concentration microdomains at squid presynaptic terminals. *Biol. Bull.* **187:** 300–303.
19. **Silver, R. B. 1989.** Nuclear envelope breakdown and mitosis in sand dollar embryos is inhibited by microinjection of calcium buffers in a calcium-reversible fashion and by antagonists of intracellular Ca^{2+}-channels. *Develop. Biol.* **131:** 11–26.
20. **Shimomura, O., B. Musicki, and Y. Kishi. 1989.** Semi-synthetic aequorins with improved sensitivity to Ca^{2+} ions. *Biochem. J.* **261:** 913–920.
21. **Shimomura, O., S. Inouye, B. Musicki, and Y. Kishi. 1990.** Recombinant aequorin and semi-synthetic recombinant aequorins. *Biochem. J.* **270:** 309–312.
22. **Inoué, S. 1986.** *Video Microscopy.* Plenum Press, New York. Pp. 149–262.
23. **Wayne, R. P. 1988.** *Principles and Applications of Photochemistry.* Oxford Science Publications, Oxford University Press, Oxford. Pp. 66–84.
24. **Hamamatsu Photonics K. K., Electron Tube Center. 1991.** *Image Intensifiers.* Shizuoka-ken, Japan.